

Sub 400 nm spatial resolution extreme ultraviolet holography with a table top laser

P. W. Wachulak, R. A. Bartels, M. C. Marconi, C. S. Menoni, and J. J. Rocca

NSF ERC for Extreme Ultraviolet Science & Technology and Department of Electrical and Computer Engineering, Colorado State University, USA

Y. Lu, and B. Parkinson

Department of Chemistry, Colorado State University, USA

Abstract: We report sub-400 nm spatial resolution with Gabor holography obtained using a highly coherent table top 46.9 nm laser. The hologram was recorded in high resolution photoresist and subsequently digitized with an atomic force microscope. The final image was numerically reconstructed with a Fresnel propagator. Optimal reconstruction parameters and quantification of spatial resolution were obtained with a wavelet analysis and image correlation.

©2006 Optical Society of America

OCIS codes: (090.0090) Holography; (100.2960) Image analysis

References and Links

1. D. Gabor, "A new microscopic principle," *Nature* **161**, 777 (1948).
2. E. N. Leith and J. Upatnieks, "Reconstructed wavefronts and communication theory," *J. Opt. Soc. Am.* **52**, 1123 (1962).
3. A. V. Baez. "A study in diffraction microscopy with special reference to X-rays," *J. Opt. Soc. Am.* **42**, 756 (1952).
4. J. W. Giles. "Image reconstruction from a Fraunhofer X-ray hologram with visible light," *J. Opt. Soc. Am.* **59**, 1179 (1969).
5. S. Aoki and S. Kikuta, "X ray holographic microscopy," *Jpn. J. Appl. Phys.* **13**, 1385 (1974).
6. J. E. Trebes, S. B. Brown, E. M. Campbell, D. L. Matthews, D. G. Nilson, G. F. Stone, and D. A. Whelan, "Demonstration of X-Ray holography with an X-Ray laser," *Science* **238**, 517 (1987).
7. S. Lindaas, M. Howells, C. Jacobsen and A. Kalinovsky, "X-ray holographic microscopy by means of photoresist recording and atomic force microscope readout," *J. Opt. Soc. Am. A* **13**, 1788 (1996).
8. I. McNulty, J. Kirz, C. Jacobsen, E. Anderson, M. R. Howells, and D. P. Kern, "High resolution imaging by Fourier Transform X-ray holography," *Science* **256**, 1009 (1992).
9. S. Elsebitt, W. F. Schlotter, M. Lorgen, O. Hellwig, W. Eberhardt, J. Stohr, "Lensless imaging of magnetic nanostructures by x-ray spectro holography," *Nature* **432**, 885 (2004).
10. C. D. Macchietto, B. R. Benware and J. J. Rocca, "Generation of millijoule-level soft-X ray laser pulses at a 4-Hz repetition rate in a highly saturated tabletop capillary discharge amplifier," *Opt. Lett.* **24**, 1115 (1999).
11. B. M. Luther, Y. Wang, M. A. Larotonda, D. Alessi, M. Berril, J. J. Rocca, J. Dunn, R. Keenan, V. Shlyaptsev, "High repetition rate collisional soft X-ray lasers based on grazing incidence pumping," *IEEE J. Quantum Electron* **42**, 4 (2006).
12. R. A. Bartels, P. A. Green, H. Kapteyn, M. Murnane, S. Backus, I. P. Christov, D. Attwood, and C. Jacobsen. "Generation of spatially coherent light at extreme ultraviolet wavelengths," *Science* **297**, 376 (2002).
13. G. L. Rogers. "Gabor diffraction microscopy. The hologram as a generalized zone-plate," *Nature* **166**, 236 (1950).
14. D. Attwood, *Soft X-ray and extreme ultraviolet radiation*, (Cambridge University Press. 1999).
15. Y. Liu, M. Seminario, F. G. Tomasel, C. Chang, J. J. Rocca, and D. T. Attwood, "Achievement of essentially full spatial coherence in a high-average-power soft-x-ray laser," *Phys. Rev. A*, 6303(3) art. no.-033802.
16. M. C. Marconi, J. L. A. Chilla, C. H. Moreno, B. R. Benware and J. J. Rocca, "Measurement of the spatial coherence buildup in a discharge pumped table-top soft x-ray laser," *Phys. Rev. Lett.* **79**, 2799 (1997).
17. B. R. Benware, C. H. Moreno, D. J. Burd, and J. J. Rocca, "Operation and output pulse characteristics of an extremely compact capillary-discharge tabletop soft-x-ray laser," *Opt. Lett.* **22**, 796 (1997).
18. AFM cantilever from MicroMasch with the following physical characteristics: cantilever length 230 μm , width 40 μm , thickness $t = 7 \mu\text{m}$, full tip cone angle 30° , tip height $h = 20 - 25 \mu\text{m}$, typical tip curvature radius of uncoated probe $< 10 \text{ nm}$.

19. T. Beetz and C. Jacobsen, "Soft X-ray radiation damage studies in PMMA using a cryo-STXM," *J. Synchrotron Radiat.* **10**, 280 (2002).
 20. X. Zhang, C. Jacobsen, S. Lindaas, and S. Williams, "Exposure strategies for PMMA in situ x-ray absorption near edge structure spectroscopy," *J. Vac. Sci. Technol. B* **13**, 1477 (1995).
 21. J. W. Goodman, *Introduction to Fourier Optics*, (Roberts and Company Publishers, 2005).
 22. J. Nuñez, X. Otazu, and M. T. Merino, "A multiresolution-based method for the determination of the relative resolution between images: First application to remote sensing and medical images," *Int. J. Imaging Syst. Technol.* **15**, 225 (2005).
-

1. Introduction

Holographic imaging was introduced by Gabor in 1948 [1]. However, holography was not widely practiced until Leith and Upatnieks demonstrated off-axis holography in the early 1960s [2]. Extension of holographic techniques to the X-ray region was suggested several years later by Baez [3]. Nevertheless, realization of this goal proved difficult and EUV holographic images of simple objects were not obtained until the early 1970s [4, 5]. The lack of sufficiently bright coherent sources at short wavelengths was, during this period, the primary barrier to the creation of high quality holograms in this spectral region. Important advances in the field were obtained with the development of EUV lasers and synchrotron sources, which included the first demonstration of X-ray laser holography at Lawrence Livermore National Laboratory [6] using a large laser facility and achieving a spatial resolution of 5 μm . Holographic recording using X-ray radiation from synchrotrons has also been utilized for imaging biological samples [7], nano structures [8], and to study magnetic domains with nanometer resolution by the novel technique of spectro-holography [9] among other applications.

Demonstration of highly coherent compact EUV sources [10-12] enables new opportunities for the implementation of practical coherent imaging systems with nanometer-scale resolution that fit on a table-top. Recently, Gabor holographic imaging was demonstrated with a fully coherent table-top source of high order harmonic (HHG) radiation. In this initial experiment, holographic images were recorded with a EUV CCD camera. The resolution of the recording process limited the spatial resolution of the holographic imaging to approximately 7 microns [12]. In this paper, we improve the spatial resolution of table-top EUV holographic imaging to below 400 nm, representing a $\sim 17x$ improvement. An analysis details the imaging resolution of our present apparatus and is in excellent agreement with our experimental findings. This analysis provides guidance that indicates it may be possible to improve the resolution to near the diffraction limit. The paper is organized as follows: section 2 details our theoretical analysis of holographic imaging, followed by a description of the experimental setup, and finally an analysis of the imaging resolution of our experimental results.

2. Spatial resolution of coherent holographic imaging systems

The hologram formed by a point object is equivalent to a Fresnel zone plate (FZP). Rogers [13] demonstrated that the implication of this fact is that holograms formed from complex objects may be regarded as a superposition of FZPs. The resolution of the holographic imaging process is consequentially identical to that of imaging with FZP lenses. As with any imaging system, the resolution of the process is dictated by the numerical aperture (NA) of the imaging system. The NA and thus the imaging resolution of FZP lenses is set by the outermost zone width [14]. With holography, the resolution of the recording medium is one factor that limits the NA of the FZPs formed in the interferogram. Following the work of Lindaas et. al. [7], we record our holograms in high-resolution photoresist. Provided that the incident reference beam overlaps with all of the scattered light from the object, the geometry of the experiment does not degrade the hologram NA. Under these conditions, the NA of the recording stage of holographic imaging is dominated by the spatial and temporal coherence of the EUV laser source. Moreover, the holograms are digitized with an AFM, thus the digitization may also limit the spatial resolution of the process.

The temporal and spatial coherence of the illumination source limit the hologram NA when the path difference between the radiation scattered by the object and the reference beam exceeds either the longitudinal or transverse coherence lengths. As a consequence, the Rayleigh spatial resolution given by $\Delta = (0.61 \lambda)/NA$ where λ is the wavelength of the illumination is limited by the source coherence. The numerical aperture of the hologram for a laser source with a longitudinal coherence length given by $l_c = \lambda^2/\Delta\lambda$ is restricted to

$$NA = \left[\frac{l_c}{z_p} \right]^{1/2} \quad (1)$$

where z_p defines the distance from the object to the recording medium. This restriction of the hologram NA in the recording phase translates into a Rayleigh-limited image spatial resolution of

$$\Delta = 0.61 \lambda \left[\frac{z_p}{l_c} \right]^{1/2} = 0.61 \left[z_p \Delta\lambda \right]^{1/2} \cdot \quad (2)$$

For the geometry used in this work in which the object-recording medium distance was set to $z_p = 4$ mm, and using $\Delta\lambda/\lambda = 1 \times 10^{-4}$ for the 46.9 nm laser, the temporal coherence limits the $NA \approx 0.342$, limiting the image spatial resolution to $\Delta \approx 84$ nm.

Similarly, the source spatial coherence limits the numerical aperture of the hologram to $NA = R_c/z_p$, where R_c is the transverse coherence radius of the EUV laser at the object plane. The coherence radius of the discharge pumped 46.9 nm laser equipped with a capillary 18.4 cm long as used in this experiment is approximately $R_c \approx 340$ μm at the object plane located at $z_s = 1.70$ m from the laser. This coherence radius limits the $NA = 0.085$, yielding a spatial resolution of $\Delta \approx 338$ nm. The spatial coherence can be improved however by using a longer laser capillary [15, 16] which simultaneously increases the energy per pulse [17].

In order to reconstruct the holographic image, the holographic interferogram recorded in photoresist was digitized by an atomic force microscope (AFM). Given the relationship between NA and outer zone spacing Δr of an FZP [14], the minimum number of samples required to satisfy the Nyquist sampling criterion for a given spatial resolution is $N_{sample} = 2D/\Delta r$, where D is the size of the hologram. This can be related to the image resolution by $N_{sample} = (2.98 \lambda z_p) / \Delta^2$. Clearly, the total number of sampling points for the two dimensional interferogram, $(N_{sample})^2$, necessary to attain a given holographic imaging resolution becomes excessively large if the object-recording medium distance z_p is not kept small.

Based on the consideration outlined above, in our experiment the primary constraint on realizing high resolution EUV Gabor holographic imaging is the interferogram sampling. To appreciate this point, let us consider the case in which we set the imaging resolution to $\Delta \approx \lambda$, and $N_{sample} = 3000$ as used in the AFM reading of the hologram image discussed in the next section. For these conditions, the object-recording medium distance must be set to $z_p = 58$ μm in order to achieve wavelength limited resolution. This value of z_p contrasts with values of $z_p = 560$ μm and $z_p = 1260$ μm that are required to attain wavelength-limited imaging resolution when considering the effects of spatial and temporal coherence, respectively, of the EUV laser source used in this work.

3. Experimental details

The experimental set up is schematically illustrated in Fig. 1. The 46.9 nm wavelength light used for illumination is produced by a table top discharge pumped capillary Ne-like Ar laser. This compact laser when operated with 18.4 cm long capillaries produced 0.1 μJ pulses at a repetition rate of 1 Hz [17] and occupies a compact $1 \times 0.5 \text{ m}^2$ footprint. The EUV laser has a high temporal coherence with a fractional spectral bandwidth of $\Delta\lambda/\lambda \approx 1 \times 10^{-4}$, which corresponds to a coherence length of $l_c \approx 470 \mu\text{m}$. This high longitudinal coherence allows the recording of larger NA holograms, increasing the achievable spatial resolution as compared with other EUV table top sources [12] for the same recording conditions.

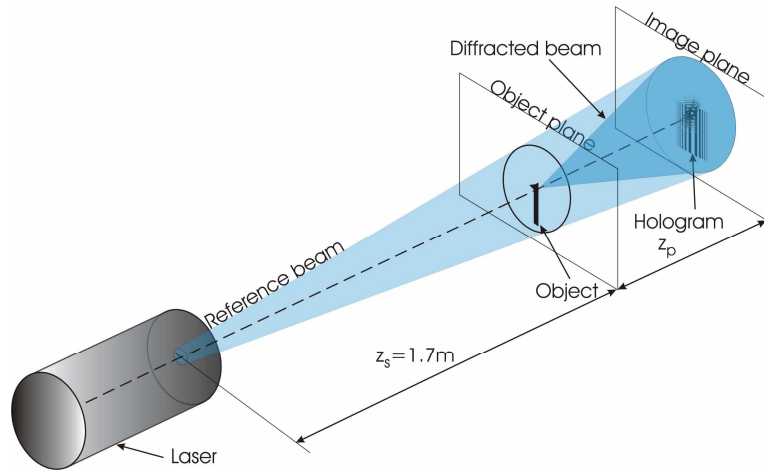


Fig. 1. Scheme of the experimental set up.

An AFM cantilever [18] served as the test object. Holograms were recorded in a 200 nm thick layer of PMMA (MicroChem 950,000 molecular weight) spin-coated on a silicon wafer. The PMMA coated wafer was situated at a distance of $z_p \approx 4 \text{ mm}$ away from the AFM cantilever to record the hologram. As shown in photon-activated experiments [7], the PMMA has a resolution similar to the EUV wavelength and thus it does not limit the spatial resolution of the holographic imaging process.

To activate the PMMA, typical exposures in the range $\approx 2 \times 10^7$ photons μm^{-2} were necessary which corresponds to a dose in the range $\approx 3\text{-}4 \times 10^6$ Gy [19,20]. Exposures of this magnitude required approximately 150 laser shots with the experimental set up utilized in this work. It would be possible to significantly reduce the exposure time by using longer capillaries that provide higher energy per pulse (up to 0.8 mJ for 36 cm capillaries) [10]. After the exposure, the photoresist was developed using the standard procedure. The sample was immersed in a solution of MIBK-methyl isobutyl ketone (4-Methyl-2-Pentanone) with IPA-isopropyl alcohol 1:1 for 30 seconds and in a 1:3 solution for 30 seconds. After that the sample was dried using compressed nitrogen.

4. Results

To obtain an image of the hologram we followed the approach of Lindaas *et al.* [7] utilizing an atomic force microscope to digitize the hologram. We used a Veeco Nanoscope III model NS3a AFM in tapping mode for the digitization. The maximum scan area allowed by this AFM is $100 \times 100 \mu\text{m}^2$. In the digitized hologram interference fringes are visible over large areas, several hundreds of microns away from the central image of the tip. As the smallest

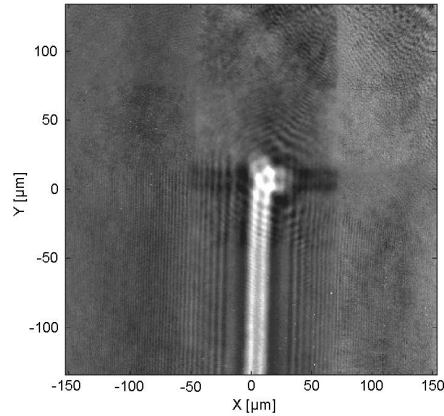


Fig. 2. Hologram read with an atomic force microscope. The image is composed by 9 sub scans to cover a total area $270 \times 290 \mu\text{m}^2$.

period interference fringes are located further away from the object, we developed a procedure that consisted of scanning different partially superposed regions of the hologram and stitching the images together to cover a larger surface. The final digitized interferogram image covering a total area of $270 \times 290 \mu\text{m}^2$ composed by 9 sub-scans is shown in Fig. 2. Larger images can be assembled increasing the number of sub-scans but with the consequent inconvenience in composing the final image with a larger number of sub-scans.

The digitized hologram was numerically reconstructed with a Fresnel propagator [21]. A plane wave was back-propagated by the FZP of focal length given by

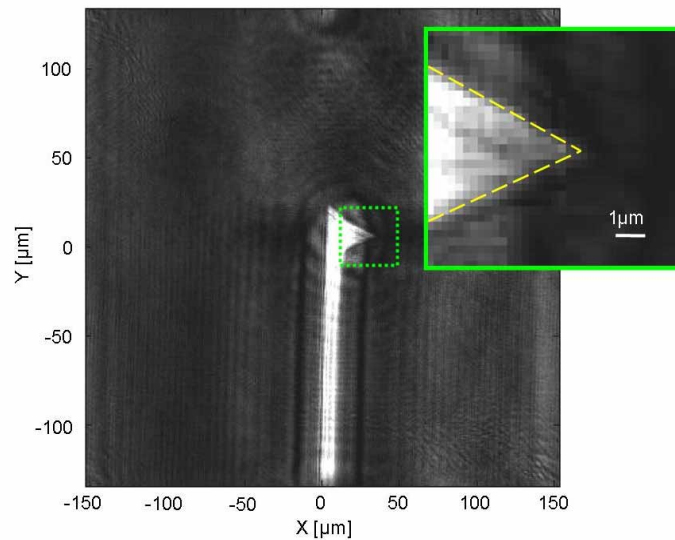


Fig. 3. Numerical reconstruction of the hologram obtained with the Fresnel propagator. The inset shows details of the cantilever tip profile.

$$\frac{1}{f} = \frac{1}{z_p} - \frac{1}{(z_s + z_p)} \quad (3)$$

and rescaled by the geometric magnification $M_g = (z_s + z_p) / z_s$ of the object as it is projected onto the holographic recording medium [12]. In these expressions z_s is the distance between the laser and the object, as indicated in the schematic shown in Fig. 1. Figure 3 is the reconstructed image obtained after processing the AFM image shown in Fig. 2 with the Fresnel propagator code. The cantilever profile is clearly displayed and the tip is obviously revealed. The inset in the figure is a magnified section of the final image where 1 pixel corresponds to 270 nm.

5. Analysis of the spatial resolution of the holographic images

When reconstructing the image from the digitized hologram, one input parameter in the reconstructing code is the distance z_p . Slight changes in z_p produce subtle variations in the reconstructed image. To quantify the spatial resolution of the reconstructed images as well as to find the optimum z_p we used a wavelet decomposition analysis followed by correlation of the reconstructed images with the wavelet set in a similar way as described by J. Nuñez et al [22]. The optimum resolution was set by a “perfect” synthesized image that was used as the reference image. This reference image was constructed to have the maximum resolution attainable, equivalent to 1 pixel. From this reference image we generated a set of lower resolution images (wavelet components) obtained by wavelet decomposition, each one having a relative resolution to the reference given by $Y = 2^X$, where Y is the relative resolution between the images in the wavelet decomposition and X is the scale of the wavelet.

The reconstructed images obtained by running the Fresnel propagator code with slightly different z_p around 4 mm were in turn correlated with this set of decreasing resolution wavelet components. The correlations between the wavelet components and the images for different z_p provide a quantitative relative resolution of these images relative to the synthesized reference image. This procedure also allows for the selection of the optimum z_p parameter. Figure 4 shows curves plotting the values of the correlation between the reconstructed images and the wavelet components as a function of the wavelet scale for different object-hologram distances ranging from $z_p = 4$ mm to $z_p = 4.08$ mm. The

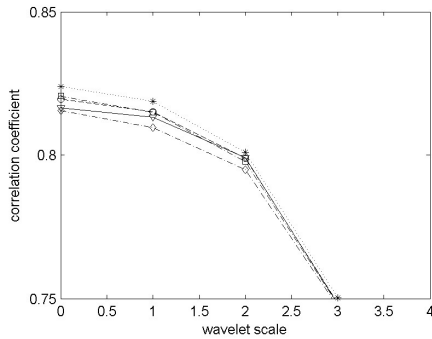


Fig. 4. Coefficient obtained from the correlation between different images reconstructed with different object-hologram distances and different wavelet components as a function of the wavelet scale. Triangles: $z_p = 4$ mm; circles: $z_p = 4.02$ mm; stars: $z_p = 4.05$ mm; squares: $z_p = 4.06$ mm; diamonds: $z_p = 4.08$ mm.

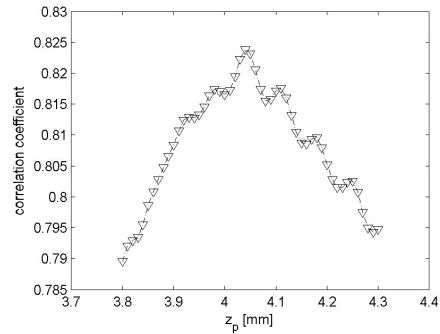


Fig. 5. Maximum correlation coefficient for images reconstructed with different object-hologram distances. The best resolution is obtained for $z_p = 4.04$ mm.

curves indicate that the largest value of the correlation function for all z_p corresponds to the wavelet scale $X = 0$, having an almost constant value in the interval $X = 0$ to $X = 1$ and decreasing faster for higher wavelet scale values. If we take the conservative assumption that the best correlation curve corresponds to $X = 0.5$, this analysis indicates a resolution $2^{0.5} = 1.41$ relative to the reference image. As the synthesized reference image has by definition 1 pixel resolution (270 nm) this analysis indicates that the reconstructed image has a resolution equivalent to 1.41 pixels.

To highlight the sensitivity of the analysis to the choice of z_p , we have plotted in Fig. 5 the maximum value of the correlation function obtained for different object-hologram distances in the 3.8 mm to 4.3 mm range. The maximum value is obtained for $z_p = 4.04$ mm. The position of the reference image relative to the reconstructed images also influences the value of the correlation. The curve shown in Fig. 5 corresponds to the position of the reference image which maximizes the value of the correlation with the reconstructed images. Moving the reference image one pixel around this optimum position produces similar curves as presented in Fig. 5 but with lower correlation values. From this analysis, we conclude that the optimum reconstruction corresponds to a distance $z_p = 4.04$ mm and that the spatial resolution obtained in the reconstruction is 381 nm, which compares well with the predicted 338 nm resolution.

6. Conclusion

We have demonstrated sub-400 nm resolution in the recording and reconstruction of a holographic image obtained in the Gabor's geometry with a table top EUV laser. This represents more than an order of magnitude improvement relative to previous holographic microscopy with a table top EUV source. With a resolution analysis, we demonstrate that the temporal and spatial coherence of the 46.9 nm laser do not limit the *NA* of the hologram easily allowing for sub 100 nm resolution. Rather the large number of sampling points required to digitize the hologram imposes the major practical limit for achieving sub 100 nm spatial resolution. To determine the optimum reconstruction parameters and assess the spatial resolution of the holographic recording we used a wavelet analysis. Image correlation was used to determine the optimum reconstruction parameters and to quantify the spatial resolution achieved in the image. In future work, it may be possible obtain sub 100 nm holographic images with an appropriate modification to our experimental geometry. Moreover, by increasing the EUV laser energy with longer capillaries, it may be possible to produce holographic images with a single EUV laser pulse, allowing for time resolved measurements in the nanosecond scale with simultaneous sub 100 nm spatial resolution.

Acknowledgments

This research was sponsored by the National Science Foundation through the NSF ERC Center for Extreme Ultraviolet Science and Technology, NSF Award No. EEC-0310717.